coatings

MDPI

Article

Solution-Processed All-Solid-State Electrochromic Devices Based on SnO_2/NiO doped with Tin

Gieun Kim, Songeun Hong, Suho Yoo and Jongwoon Park *

School of Electrical, Electronics & Communication Engineering, Korea University of Technology and Education, Cheonan 31253, Korea; rlarldmsrns@koreatech.ac.kr (G.K.); songeun629@koreatech.ac.kr (S.H.); shyoo73@koreatech.ac.kr (S.Y.)
* Correspondence: pjwup@koreatech.ac.kr

Abstract: We investigated the photochromic (PC) and electrochromic (EC) properties of tin-doped nickel oxide (NiO) thin films for solution-processable all-solid-state EC devices. The PC effect is shown to be enhanced by the addition of Sn into the precursor NiO solution. We fabricated an EC device with six layers—ITO/TiO_2 (counter electrode)/SnO_2 (ion-conducting layer)/SiO_2 (barrier)/NiO doped with tin (EC layer)/ITO—by a hybrid fabrication process (sputtering for ITO and TiO_2, sol–gel spin coating for SnO_2 and NiO). The EC effect was also observed to be improved with the Sn-doped NiO layer. It was demonstrated that UV/O_3 treatment is one of the critical processes that determine the EC performance of the hydroxide ion-based device. UV/O_3 treatment generates hydroxide ions, induces phase separation from a single mixture of SnO_2 and silicone oil, and improves the surface morphology of the films, thereby boosting the performance of EC devices. EC performance can be enhanced further by optimizing the thickness of TiO_2 and SiO_2 layers. Specifically, the SiO_2 barrier blocks the transport of charges, bringing in an increase in anodic coloration. We achieved the transmittance modulation of 38.3% and the coloration efficiency of 39.7 cm^2/C. We also evaluated the heat resistance of the all-solid-state EC device and found that the transmittance modulation was decreased by 36% from its initial value at 100 °C. Furthermore, we demonstrated that a large-area EC device can be fabricated using slot-die coating without much compromise on EC performance.

Keywords: all-solid-state; electrochromic devices; nickel oxide; tin dioxide; sol-gel process

Citation: Kim, G.; Hong, S.; Yoo, S.; Park, J. Solution-Processed All-Solid-State Electrochromic Devices Based on SnO_2/NiO doped with Tin. *Coatings* **2021**, *11*, 1431. https://doi.org/10.3390/coatings11111431

Academic Editor: Emmanuel Koudoumas

Received: 26 October 2021
Accepted: 21 November 2021
Published: 22 November 2021

1. Introduction

Chromic phenomena such as thermochromism, photochromism, electrochromism, and solvatochromism occur in a material by various external stimuli [1]. Of those, photochromism (PC) can change its optical properties reversibly through interactions with sunlight or UV radiation, and electrochromism (EC) can be obtained through redox reaction under electric field [2,3]. The former phenomenon is commercially applicable in ophthalmics, sensors, optical memory, and switches, and the latter phenomenon is still extensively studied for the applications of car mirrors, smart windows, transparent displays, and solar protection. A typical EC device requires liquid- or gel-type electrolytes due to the inherent advantage of high diffusion rates of ions through fluids. Since the incorporation of those electrolytes may have the issue of leakage and durability, or a limitation in fabricating large-area devices, all-solid-state EC devices are highly demanded for practical applications [4]. A typical all-solid-state EC device consists of a transparent electrode/ion-storage layer/ion-conducting layer(solid-state electrolyte)/EC layer/transparent electrode [5]. For the ion-storage layer serving as a counter electrode, IrO_2, TiO_2-V_2O_5, TiO_2-CeO_2, and Li_2O-FeO were used [6,7]. For the ion-conducting layer (solid-state electrolytes), ZrP, Ta_2O_5, TiO_2, ZrO_2, $LiNbO_3$, $LiAlF_4$, and LiBSO were usually employed [8,9]. EC materials can be divided into two types: anodically coloring materials (NiO, IrO_2, Cr_2O_5, etc.) and cathodically coloring materials (WO_3, MoO_3, TiO_2, Nb_2O_5, etc.) [10,11]. Of those, NiO

and WO_3 have been intensively investigated because of their high coloration efficiency, low material cost, excellent durability, and electrochemical stability [12,13]. EC devices with NiO and WO_3 have great benefits in terms of energy savings because of low driving voltage (0–5 VDC), low power consumption, and memory effect by bistability even after the power supply is disconnected [14–17].

Of many all-solid-state EC devices, a Li^+ ion-based device consisting of ITO/WO_3/LiBSO/NiO/ITO was reported by Yang et al., which exhibited the transmittance modulation (ΔT) of 52.2% and response time of 8 s and 20 s for bleaching and coloring, respectively [18]. Song et al. fabricated an all-solid-state EC device having the structure of ITO/NiO/$LiTaO_3$/WO_3/ITO. It showed an excellent transmittance modulation exceeding 67% and response time of 42 s and 85 s for bleaching and coloring states [19]. Moreover, Li et al. reported a novel four-layered structure of ITO/Li-NiO/Li-WO_3/ITO fabricated using thermal evaporation to inject lithium ions, which had the modulation of 32% and response time of 1.7 s and 8.6 s for bleaching and coloring [20]. Yoshimura et al. introduced a H^+ ion-based EC device where a thin SiO_2 film embedded between WO_3 (EC layer) and Ta_2O_5 (solid electrolyte) enhanced not only the transmittance modulation but also the response speed, all of which were fabricated by a sputter in vacuum [21]. Wang et al. prepared an all-solid-state EC device as a multilayer structure of ITO/WO_3/Ta_2O_5/NiO/ITO and the maximum ΔT was 56.7% [22]. So far, most all-solid-state EC devices are based on Li^+ or H^+ ions using solid electrolytes. There has been some research on all-solid-state EC devices based on the hydroxide ion (OH^-) [23]. The EC effect occurs by the reaction of hydroxide ions with NiO films. It is greatly affected by the annealing temperature, crystallinity, porous surface, and doping materials in the NiO films [24]. Namely, a porous NiO film doped with Zn, Cu, and Al exhibited higher EC performance. However, most of them were demonstrated using a KOH aqueous electrolyte. To our best knowledge, no extensive study on all-solid-state EC devices based on OH^- ions has been conducted. In this work, we investigated a hydroxide-ion-based all-solid-state EC device without any aqueous electrolyte included, which consisted of ITO/TiO_2 (counter electrode)/SnO_2 (ion-conducting layer)/SiO_2 (barrier)/NiO doped with tin (EC layer)/ITO. The EC device was fabricated using a hybrid process: sputtering deposition for transparent electrodes including TiO_2 and sol-gel deposition for SnO_2 and NiO. The sol-gel process enables large-area coatings at a relatively low temperature and cost-effective production. It also allows easy control of the doping concentration [25]. Although NiO thin films have been extensively studied in literature, the use of SnO_2 as a dopant is little investigated. It was shown that EC performance can be improved by the addition of tin (Sn) into a NiO solution due to an increase in active sites. It was found that UV/O_3 treatment applied after coatings of SnO_2 and NiO layers is the most critical process to achieve the EC effect. We also demonstrated that a UV-treated silicon oil mixed into a precursor SnO_2 solution is converted into an insulation layer between SnO_2 and NiO layers, enhancing EC performance.

2. Materials and Methods

We first fabricated a NiO film using the sol-gel process to investigate the doping effect of Sn on its PC property. Then, we fabricated all-solid-state EC devices with a Sn-doped NiO EC layer using spin and slot-die coatings.

2.1. Fabrication of Sn-Doped NiO Films for Photochromism

The NiO solution was obtained by dissolving 5 wt% of nickel acetate tetrahydrate (Sigma Aldrich, St. Louis, MO, USA, 98%) in 2-dimethylaminoethanol (Sigma Aldrich, 99.5%) for 2 hrs at 60 °C using a hotplate (MSH-20D, Daihan Scientific, Wonju, Korea). The Sn-doped NiO solutions were obtained by adding Tin(II) 2-ethylhexanoate (Sigma Aldrich, 92.5–100.0%) into the NiO solution as a dopant. The mixture was then stirred for 20 min. The solution was coated on a glass substrate as large as 25 × 25 mm^2, which was cleaned with 2-propanol anhydrous (Sigma Aldrich, 99.5%) for 15 min in an ultrasonic bath (Powersonic 410, Hwashin, Seoul, Korea). Spin coatings were performed at 3000 rpm

for 5 s, and the coated films were dried at 80 °C for 1 min and then at 115 °C for 9 min. The photochromic properties of the films were measured using UV-VIS spectrophotometer (T 70+, PG Instruments, Lutterworth, UK) and UV/O_3 Cleaner (Model 24, BESSCO, Seoul, Korea). The samples were irradiated with UV light from a mercury lamp (Jelight Inc., Irvine, CA, USA, 35 mW/cm^2, 184 nm and 254 nm wavelength) for 70 min while maintaining the plate temperature at 60 °C. The thickness and surface morphology of the NiO films were measured using scanning electron microscope (SEM, JSM-7500F, JEOL Ltd., Tokyo, Japan) and atomic force microscope (AFM, XE-100, Park Systems Corp., Suwon, Korea).

2.2. Fabrication of All-Solid-State EC Devices

Presented in Figure 1 is the layer structure and energy band diagram of the all-solid-state EC devices (six layers). The upper part of the rectangle represents the conduction band minimum and the lower part the valence band maximum, and the values below each layer represent the band gap [26]. ITO/TiO_2 serves as a counter electrode, SnO_2 acts as an ion-conducting layer, SiO_2 is a barrier layer, and Sn-doped NiO is the optically functional EC layer. The TiO_2 and anodic ITO layers were fabricated using a sputter, and the other layers were formed by the sol–gel process. TiO_2 was deposited on the ITO pre-coated glass substrate by RF magnetron sputtering (The1-MSS2, TheONE Science) using a TiO_2 target (3″ diameter × 1/8″ thickness, 99.99% purity). The base pressure was 8.0 × 10^{-6} torr. Argon was utilized as a sputtering gas with a flow rate of 15 sccm, and the working pressure was maintained at 5 × 10^{-3} torr. The distance between the target and substrate was 7 cm, and the substrate was rotated at 10 rpm. The deposition was carried out for 15 min at the power of 200 W to obtain the 83 nm thick films. Anodic ITO was deposited by direct-current (DC) magnetron sputtering using ITO target (3″ diameter × 1/8″ thickness, 99.99% purity). The flow rate of argon was 15 sccm, and the working pressure was maintained at 2 × 10^{-3} torr. The deposition was performed for 7 min at a power of 50 W, providing a 100 nm thick ITO film.

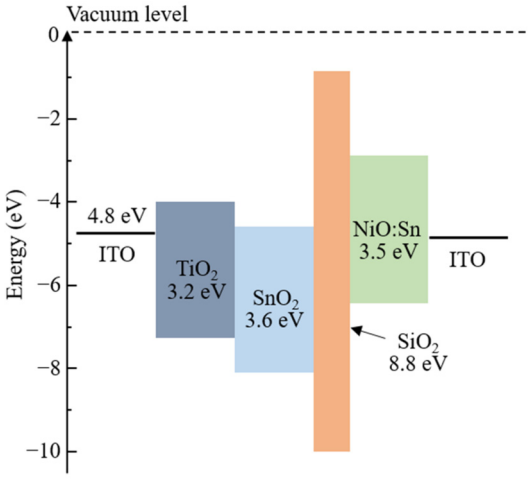

Figure 1. Layer structure and energy band diagram of all-solid-state EC device.

2.2.1. Spin Coating

As a precursor for the SnO_2 film, 22 wt% of Tin(II) 2-ethylhexanoate was dissolved in Xylene (Sigma Aldrich, 98.5%), and the mixture was stirred for 30 min at room temperature (Figure 2). In the SnO_2 solution, 3 wt% of silicone oil (Esung Materials) was added to form the SiO_2 barrier. The solution was spin-coated at 3000 rpm for 5 s onto the TiO_2 substrate, and the film was dried on the hotplate at 80 °C for 10 min. Then, the film was exposed to UV light using a UV/O_3 Cleaner for 70 min while maintaining the plate temperature at 20 °C using a chiller. NiO was deposited on the SnO_2 film in the same way described in Section 2.1.

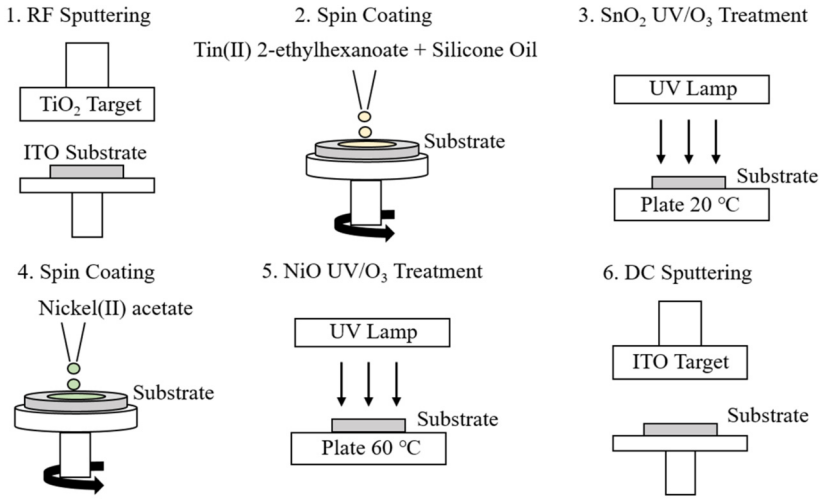

Figure 2. Fabrication process flow of all-solid-state EC device using a spin coater.

To enhance the EC properties of the devices, we fabricated them by varying different parameters such as the Sn concentration in the NiO solution, the concentration of silicon oil in the SnO_2 solution, and the TiO_2 thickness. The electrochemical property of the EC devices was measured by Autolab PGSTAT 302N potentiostat/galvanostat, and the transmittance of colored and bleached states was measured by UV-vis spectrometer within the range of 250–800 nm. The applied voltages for bleaching and coloring were set to be 0 V and 2.5 V, respectively. The layer thickness of the EC device was measured by SEM.

2.2.2. Slot Coating

To investigate the scalability to large-area EC devices, we fabricated the SnO_2 and NiO films using a table coater (TSDC-KTEU, DCN), as shown in Figure 3. The table slot coater consists of a moving plate (400 mm × 500 mm) with a plate heater (up to 150 °C), dry unit (NIR lamp up to 400 °C), syringe pump system (flow rate 0.1~10 mL/min), and slot head module (head size: 40 mm × 30 mm × 105 mm, lip length: 20 mm, surface flatness: ±3 μm, coating gap: 3~2000 μm with a resolution of 1 μm). In the slot-die head with the effective coating width of 20 mm, a shim with the thickness of 25 μm was embedded, which was fabricated using a polyimide (PI) film by a laser cutter. To obtain the same layer thickness as fabricated by spin coating, we increased the weight percentage of Tin(II) 2-ethylhexanoate in the SnO_2 solution to 30 wt%, doubled the weight percentage of Nickel(II) acetate tetrahydrate and Tin(II) 2-ethylhexanoate in the NiO solution (the ratio of them remained unchanged), and then performed slot coatings at the coating speed of 5 mm/s, coating gap of 200 μm, and flow rate of 0.02 mL/min.

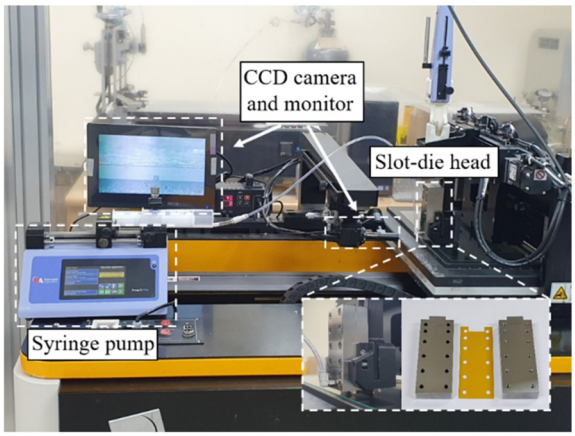

Figure 3. Image of a table slot-die coater and slot-die head used for experiments.

3. Results

3.1. Photochromic Properties of Sn-Doped NiO Films

We first investigated the photochromic property of the undoped NiO thin film fabricated on a bare glass substrate. As seen in Figure 4, the undoped NiO film exhibits the transmittance of 92% at a wavelength of 550 nm before UV/O_3 irradiation, but it is reduced to 85% after UV/O_3 treatment. The color of the film was changed to brown, indicating the emergence of the photochromic effect (transmittance modulation of 7%). Photochromism in WO_3 is known to be connected to optically excited electron (e^-)-hole (h^+) pairs, which can decompose water incorporated in WO_3 [27]. The light-induced decomposition of H_2O can be written as $H_2O + 2h^+ \Leftrightarrow O + 2H^+$. The protons together with the optically excited electrons lead to the formation of colored tungsten bronze H_xWO_3. Meanwhile, the photochromic effect in NiO can be explained as follows [28,29]. Moisture residing on the thin films during UV/O_3 irradiation is decomposed into OH^- and O_2 (Equation (1)). The hydroxide ions react with the NiO film, causing NiOOH that is colored into brown (Equation (2)) [30].

$$O_3(H_2O) + hv \rightarrow 2OH^- + O_2 \quad (1)$$

$$NiO + OH^- \rightarrow NiOOH + e^- \quad (2)$$

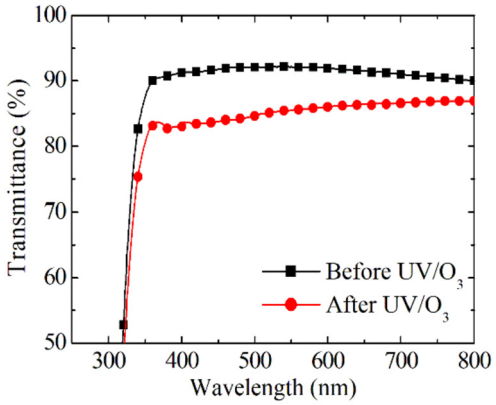

Figure 4. UV-vis spectra of undoped NiO film before and after 70 min UV/O_3 irradiation.

It is well known that UV/O_3 treatment reduces the surface energy (change contact angle) of thin films, shifts the Fermi level upward (band alignment), and increases the conductivity of films (i.e., quality of films). As such, it is likely that the UV-treated NiO films have more hydroxyl groups (-OH) involved in oxidization and reduction processes, inducing the photochromic effect. In addition, UV/O_3 treatment brings in the sintering effect [31], making the NiO films denser and more uniform. To confirm it, we measured the thickness of NiO films before and after UV/O_3 treatment using SEM. As evident in Figure 5, the film thickness was 122 nm before UV/O_3 treatment, whereas it was reduced to 50 nm after UV/O_3 treatment. Such a dense film is expected to enhance the film conductivity. Although the sintering effect would also appear by thermal annealing, it may degrade the device performance if the annealing temperature is too high (affecting the underlying layers). Therefore, UV/O_3 treatment is preferred because it can be performed at a relatively low temperature.

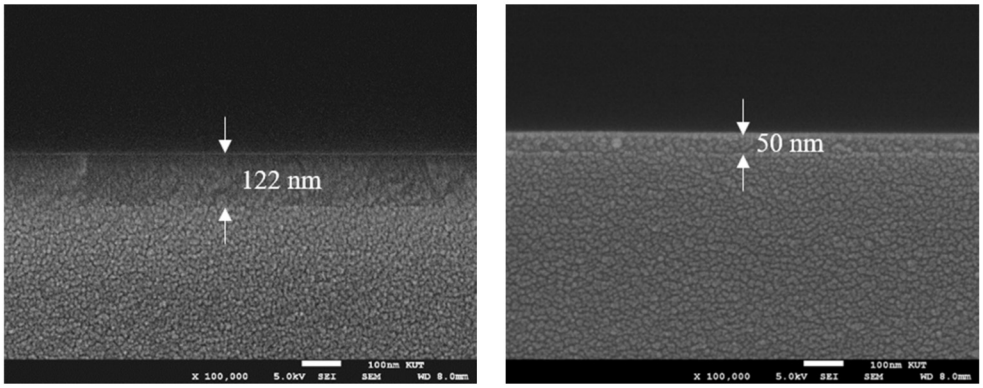

(**a**) (**b**)

Figure 5. SEM images of undoped NiO film (**a**) before and (**b**) after UV/O_3 treatment.

To further enhance the PC effect of the NiO film, we doped Sn into the NiO solution. The doping concentration was varied within the range of between 0.5 wt% and 3 wt%. Presented in Figure 6a are the transmittance spectra of Sn-doped NiO films and in Figure 6b the images of the color change of those films after UV irradiation. At a doping concentration of 2 wt%, we achieved the lowest optical transmittance (63% at 550 nm). By the addition of Sn, the transmittance modulation was improved by 22% (7% to 29%) compared with the undoped NiO film. The enhancement in the PC effect can be explained using the band diagram of NiO, as depicted in Figure 7. Under UV irradiation, electrons are excited from the valence band to the conduction band and then move to the lower side formed by the addition of Sn, where they are more stable. Since NiO is the anodically coloring material, it is colored by charge ejection (oxidization process). By the addition of Sn, such an oxidization process becomes more pronounced, causing an increase in the transmittance modulation. A similar effect can be found in [32], which demonstrated that enhancement of charge-transfer kinetics and cyclic stability can be achieved for complementary WO_3-NiO electrochromic devices by incorporating a thin SnO_x (~5 nm) interfacial layer. By the doping of Sn, the Fermi level (E_F) shifts toward the conduction band of NiO [33].

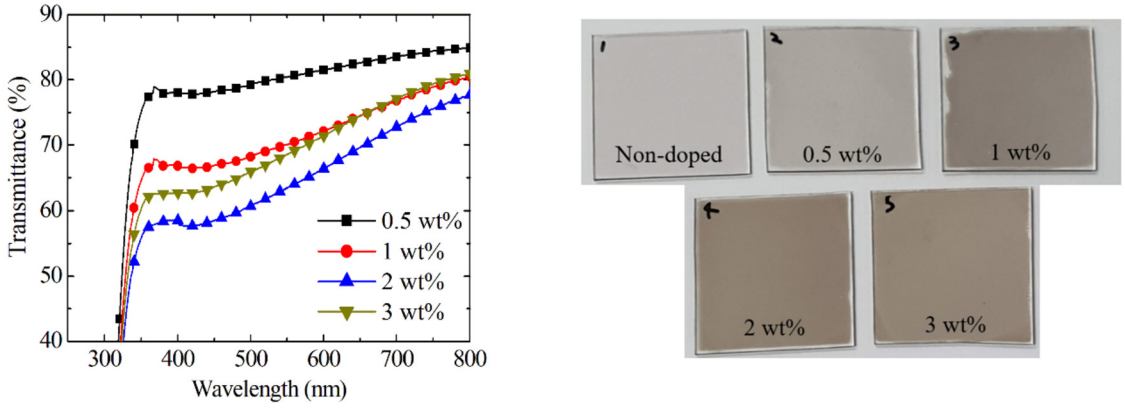

(**a**) (**b**)

Figure 6. (**a**) Transmittance spectra and (**b**) images of Sn-doped NiO films for different Sn concentrations after 70 min UV/O_3 treatment.

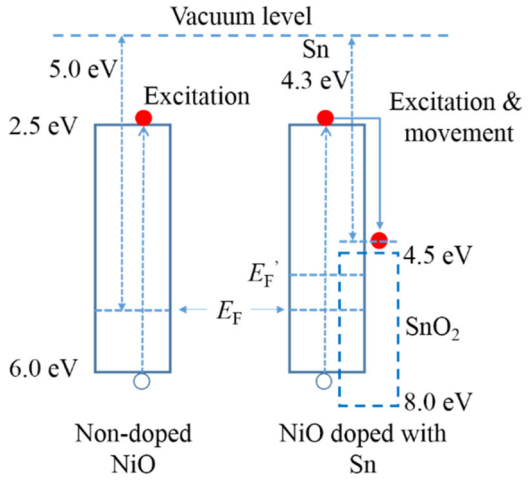

Figure 7. Energy band diagram showing the effect of Sn doping into NiO.

Figure 8 shows the transmittance spectra of 2 wt% Sn-doped NiO films as a function of UV/O_3 irradiation time. When the irradiation time was between 40 and 60 min, a big change in the optical transmittance was observed in the PC effect. Based on this result, we chose the optimum UV irradiation time to be 70 min in the fabrication of the EC device. The doping of Sn also affects the surface morphology of the NiO films. To confirm this, we measured their X-ray diffraction (XRD, Empyrean, Panalytical, Malvern, UK) and surface roughness values and present the results in Figure 9. As evident in Figure 9a showing the XRD patterns of NiO films with and without UV/O_3 treatment and with 2 wt% Sn doping, no crystalline peaks were observed regardless of UV/O_3 treatment and Sn doping. Namely, NiO films with and without UV/O_3 treatment and with Sn doping were completely amorphous with no orientation. The average roughness (R_a) and peak-to-valley roughness (R_{pv}) of the undoped NiO film were measured to be 1.1 nm and 31 nm, respectively. The average roughness is the average of how far each point on the surface deviates in height from the mean height, and the peak-to-valley roughness value measures the maximum depth of the surface irregularities. They affect the stability of the device because the short-circuit phenomenon would occur if those values were too high compared with the layer thickness. By the addition of 2 wt% Sn, the R_a and R_{pv} values were reduced to 0.7 nm and 21 nm, respectively. Namely, the surface morphology of the NiO film was enhanced with increasing Sn concentration. A similar result was also observed in [31], showing that the incorporation of the impurity (Sn) into NiO_x films annealed at lower temperatures suppressed the grain growth and thus smoother surface. From those results (Figures 6–9), it is expected that the addition of Sn into NiO would enhance the EC performance of all-solid-state devices.

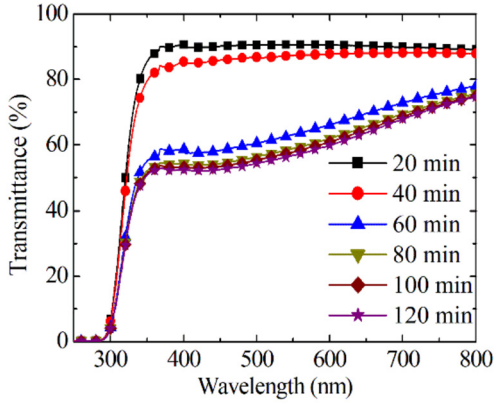

Figure 8. UV-vis spectra of 2 wt% Sn-doped NiO films for different UV/O_3 treatment times.

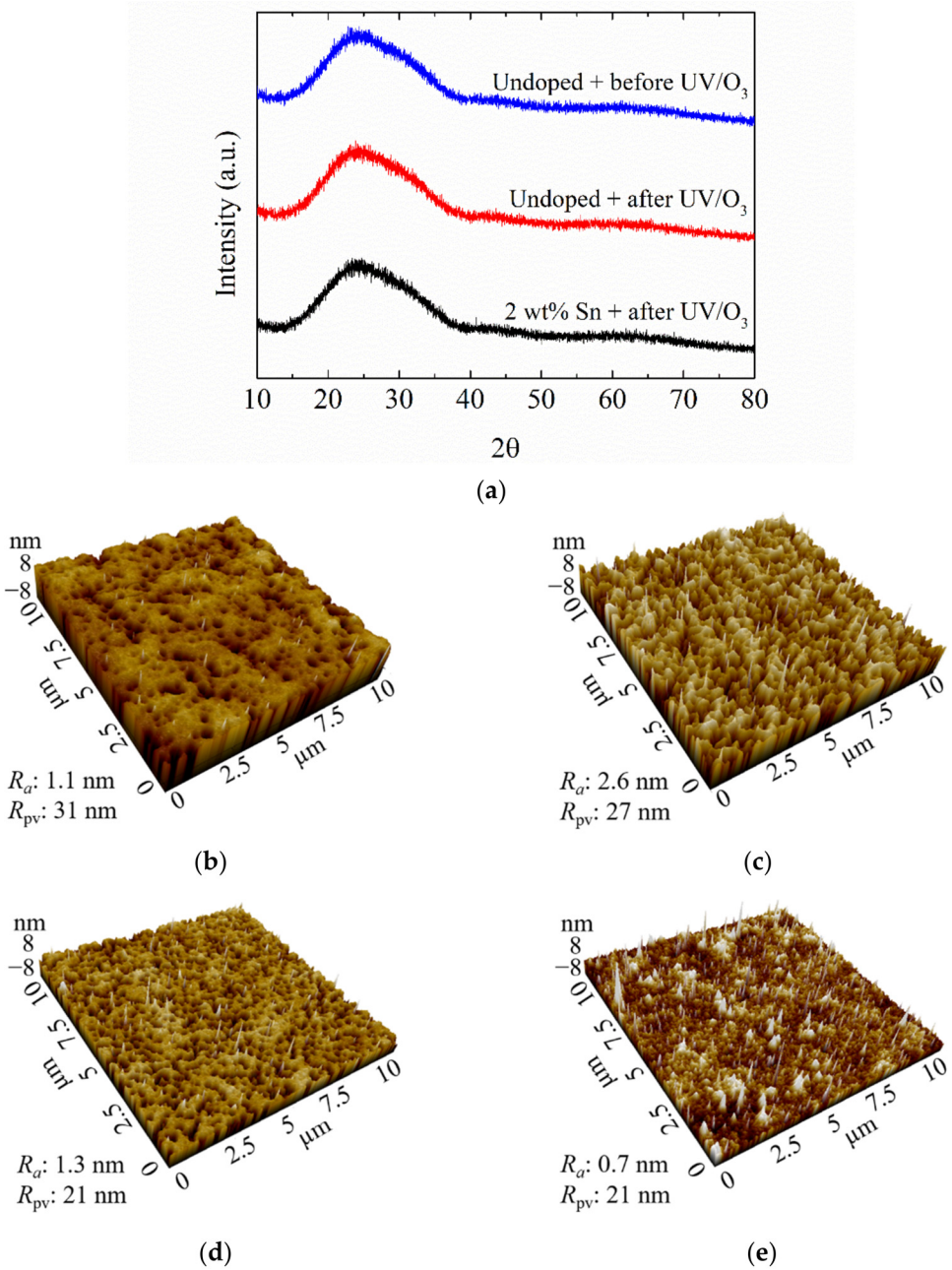

Figure 9. (**a**) XRD patterns of NiO films and AFM images of (**b**) undoped, (**c**) 0.5 wt%, (**d**) 1 wt%, and (**e**) 2 wt% Sn-doped NiO films.

3.2. Electrochromic Properties of EC Devices

Presented in Figure 10a is the SEM image showing the layer thickness of the EC device fabricated by spin coating. Even though a hybrid process (sputtering and coating) was employed to fabricate the device, each layer is shown to be well defined. The thickness of the TiO_2 and Sn-doped NiO layers was measured to be 83 nm and 32 nm, respectively. In particular, phase separation appeared during UV/O_3 irradiation from a single mixture of SnO_2 and silicone oil, causing the separated layers of SnO_2 (~62 nm) and SiO_2 (~10 nm). The thin SiO_2 layer was formed atop the SnO_2 layer. In fact, such a conversion process was applied to form the SiO_2 film [34]. It was demonstrated that ozone and atomic oxygen, produced by exposure of atmospheric oxygen to UV radiation, remove organic portions of siloxane polymers as volatile products and leave a thin silicon oxide surface film. UV/O_3 treatment removes up to 89% of the carbon from the resultant surface film, leading to an

overall stoichiometry close to that of SiO_2. Therefore, UV/O_3 treatment can also provide a facile means of generating silicon oxide films. To demonstrate its effect more clearly, we added more silicone oil (from 3 wt% to 12.5 wt%) to the precursor SnO_2 solution and spin-coated it under the same condition described in Section 2.2. As evident in Figure 10b, phase separation occurred, and the thickness of the SiO_2 layer increased to 93 nm. The thickness of the SnO_2 layer also increased because more high-viscosity (450 cSt) silicone oil was added into the precursor SnO_2 solution with the viscosity of 306 cSt, by which less solution may be expelled from the substrate during spin coating. UV/O_3 treatment may cause the photodiffusion phenomenon (the emergence of a discontinuity or discrete islands of the overcoated layer by the UV-induced diffusion process). As evident in Figure 10, however, such a phenomenon was not observed.

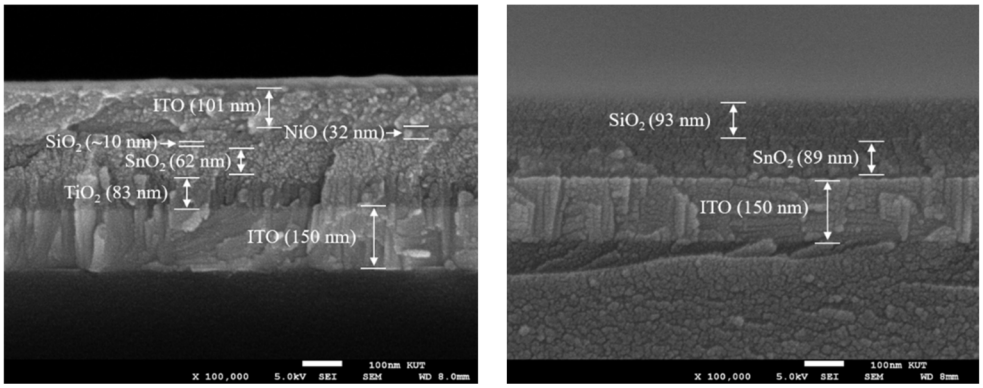

(**a**) (**b**)

Figure 10. SEM image of (**a**) the EC device with 2 wt% Sn-doped NiO layer and (**b**) SnO_2 layer on which the separated SiO_2 layer is formed after UV treatment.

We investigated the EC property of the device with the same structure as in Figure 10a. Figure 11 shows the measured transmittance spectra and response time of the EC device with a 2 wt% Sn-doped NiO film. Summarized in Table 1 is the ΔT value measured at a wavelength of 550 nm for different Sn concentrations. The ΔT value of the EC device with the undoped NiO film was as low as 5.1%, whereas it was increased to 25.7% with the 2 wt% Sn-doped NiO film, a consequence similar to the PC effect in Figure 6. We obtained a transmittance of 77.6% in the bleached state and 51.9% in the colored state at 550 nm. The insets in Figure 11a are photographs of the EC device in bleached and colored states. Compared to the PC properties, the EC device shows a dark gray color rather than brown. One may speculate that it is because the SnO_2 layer also acts as an EC layer. In fact, electrochromism was also observed in SnO_2 films, and its EC effect was sensitively dependent on their crystallinity and preferred orientations [24]. However, the EC effect was extremely low using an amorphous SnO_2 film. Furthermore, no photochromism was observed in the SnO_2 film. It seems that the dark gray color is induced by the multi-layer structure. Although there may be some EC effect by the SnO_2 layer, the NiO layer is the main EC layer. The response time for bleaching (t_b) and coloring (t_c), defined as the time required to reach 90% and 10% of the final and initial transmittance values [32], was measured to be 12 s and 20 s, respectively, as evident in Figure 11b, which is close to that (8 s for t_b and 20 s t_c) of the EC device with LiBSO. Shown in Figure 12a,b is the measured cyclic voltammogram performed between 0 V and 2.5 V at a scan rate of 100 mV/s for different Sn concentrations and optical density (ΔOD) versus charge density for the calculation of the coloration efficiency, respectively. The optical density and coloration efficiency (CE) are expressed as

$$\Delta OD = \log \frac{t_b}{t_c} \quad (3)$$

$$CE = \frac{\Delta OD}{Q_d} \quad (4)$$

where T_b is the optical transmittance in the bleached state, T_c is the transmittance in the colored state, and Q_d is the charge density. The current density (CE value) was measured to be 0.08 mA/cm^2 (3 cm^2/C) with the undoped NiO film, 0.21 mA/cm^2 (8.4 cm^2/C) with the 1 wt% Sn-doped NiO film, 0.77 mA/cm^2 (29.2 cm^2/C) with the 2 wt% Sn-doped NiO film, and 0.59 mA/cm^2 (16.3 cm^2/C) with the 3 wt% Sn-doped NiO film. Namely, the addition of dopants brings in an increment of anodic current density and thus coloration efficiency. Similar to the PC effect, the optimum amount of Sn dopant exhibiting the highest coloration efficiency was 2 wt%.

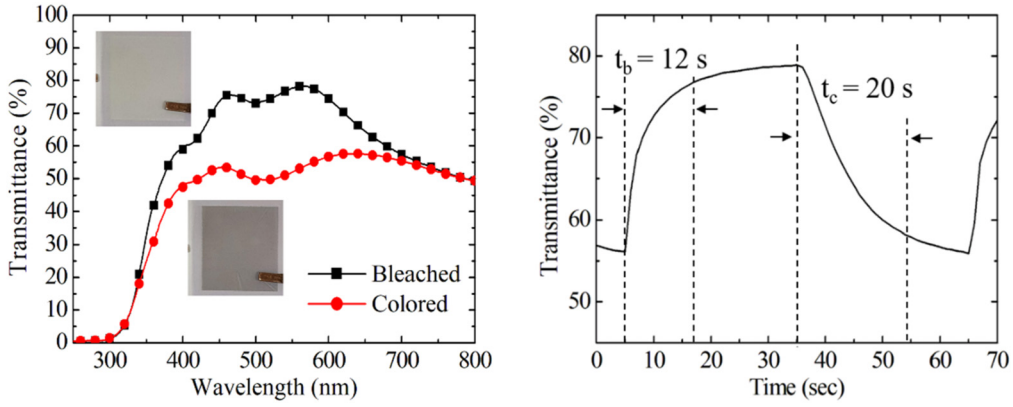

(**a**) (**b**)

Figure 11. (**a**) Transmittance spectra measured after applying a voltage for 2 min and (**b**) response time of the EC device with 2 wt% Sn-doped NiO film (the dash lines indicate the time required for the transmittance to reach 0% to 90% or 100% to 10%).

Table 1. Transmittance modulation of the EC device at 550 nm for different Sn concentrations in the NiO layer.

Sn Concentration (wt%)	ΔT (%)
Non-doped	5.1
1	20.5
2	25.7
3	21.0

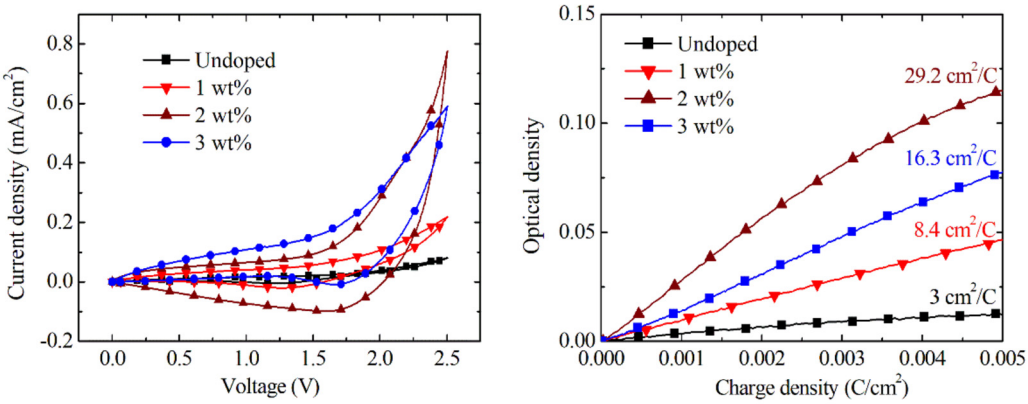

(**a**) (**b**)

Figure 12. (**a**) Measured cyclic voltammogram performed between 0 V and 2.5 V for different Sn concentrations and (**b**) optical density versus charge density for the calculation of the coloration efficiency.

As depicted in Figure 13, the SnO_2 film is an n type and the NiO film is a p type. The hydroxyl protons are generated during UV irradiation on the surface of the SnO_2 and NiO

films because UV-treated films have more hydroxyl groups (-OH) that modify the surface energy. Under a forward bias, electrons and holes are blocked by the SiO_2 barrier, causing a charge accumulation (electrons in the SnO_2 layer and holes in the NiO layer). At the same time, electrons are extracted from the NiO layer or trapped to the lower side formed by the addition of Sn (Figure 7), increasing the anodic charge density. Furthermore, the hydroxide ions are transported to the EC layer through SiO_2, and thus reaction occurs, causing anodic coloration. It is apparent that Sn doping improves EC performance (anodic coloration) due to an increase in the reaction sites in the EC layer. A similar effect was observed in the CV measurement using an aqueous electrolyte (KOH). In [23], the quantity of ions and electrons extracted from the NiO film increased with increasing doping concentration, indicating that the reaction activity of the Zn-doped NiO thin film was better than the undoped NiO film. In [35], the Al-doped NiO film also showed an increase in the anodic and cathodic peak currents. It was demonstrated that Al doping augmented the specific surface area and active sites, and a moderate amount of Al doping could be conductive for ion transport. In [25], the addition of the dopant (V_2O_5) caused a significant improvement in charge density values. The anodic charge density increased from 25.5 mC/cm^2 for the NiO film to 52.8 mC/cm^2 for the 10 mol% V_2O_5-doped NiO film. The V_2O_5-doped NiO film also improved the optical properties and kinetics of the insertion and extraction process.

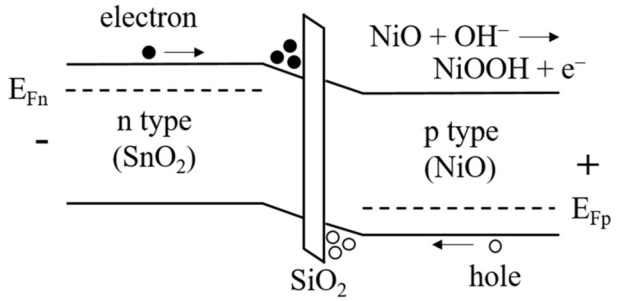

Figure 13. Energy band diagram of all-solid-state EC device with SiO_2 layer.

In our device structure, UV/O_3 treatment is one of the critical processes that determine EC performance. We found that no EC effect was observed if UV/O_3 treatment was removed even once in our fabrication process (first treatment for SnO_2 and second treatment for NiO). As discussed above, UV/O_3 treatment played a key role in phase separation, forming the separated SiO_2 layer on the SnO_2 layer. Moreover, it generated the hydroxyl protons that react with the NiO film. It also enhanced the surface morphology of the NiO film. Such positive effects that appeared in the NiO film were also observed in SnO_2 films [36]. The intensity of the -OH bond in UV/O_3-treated amorphous SnO_2 increased, compared with that in amorphous SnO_2 without UV/O_3 treatment. It indicates that the UV-treated SnO_2 films have more hydroxyl groups. Furthermore, the UV-untreated SnO_2 film had an irregular surface with distinct valleys, but the UV-treated SnO_2 film had a dense and more uniform surface. It was also demonstrated that the UV-treated SnO_2 showed better charge transport and less recombination due to the high electronic conductivity and the smooth surface [36]. The E_F of UV-treated SnO_2 was found to be shifted upward because the UV treatment affected the electron density by the formation of -OH chemisorption. Therefore, the UV/O_3-treated SnO_2 layer is expected to enhance the EC performance of the device. However, much care should be taken in selecting the UV power and time during the UV/O_3 treatment process. For the SnO_2 film, the optimum UV power and time were 35 mW/cm^2 and 70 min, which was also applied for the NiO film. When the UV power was too high or time was too long, the film was colored and never returned to its original color.

In an attempt to improve the performance of the EC device, we varied the TiO_2 layer thickness within the range of between 16 nm and 95 nm, which was done by controlling RF sputtering time. As presented in Figure 14 and Table 2, the ΔT value of the EC device was increased from 21.3% to 38.3% when the TiO_2 thickness was decreased from 95 nm to

48 nm. However, when the TiO_2 thickness was less than 48 nm, the ΔT value was rather decreased. The optical transmittance of the EC device with the 48 nm thick TiO_2 layer was 85.5% in the bleached state and 47.2% in the colored state at 550 nm. The response time for bleaching (t_b) and coloring (t_c) was measured to be 10 s and 14 s, respectively. It was observed that the response time (t_c) was reduced by about 30%, compared to the EC device with the 83 nm thick TiO_2 film in Figure 11. Since TiO_2 is not only an ion-storage layer but also an insulating material, a thick TiO_2 layer reduces the response speed of the EC device. Therefore, the optimum TiO_2 thickness in this work was observed to be about 48 nm. Through a comparison between the insets in Figures 11a and 14a, we can see that the color of the device becomes darker in the colored state when the TiO_2 layer is thinner. We also measured the chromaticity of the EC device using a spectrophotometer (ColorMate, SCINCO, Seoul, Korea) and present the result in Figure 14c. The chromaticity coordinate lies in the second quadrant (yellow-green region, a* = −8.0275, b* = 4.5311) in the bleached state, showing yellowish-green color. It shifts to the first quadrant (yellow-red region, a* = 8.0468, b* = 5.1983) in the colored state, exhibiting dark grayish-brown color.

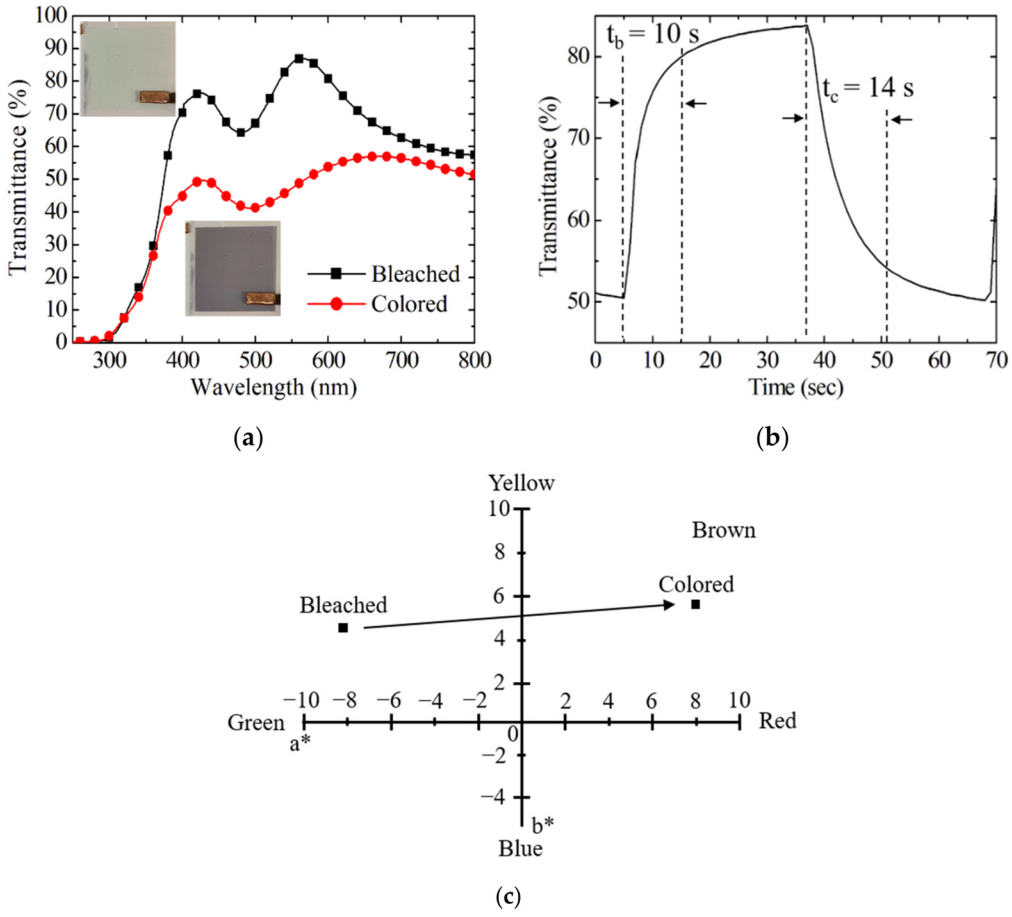

Figure 14. (**a**) Measured transmittance spectra, (**b**) response time, (**c**) chromaticity diagram of the EC device with 48 nm thick TiO_2 layer.

Table 2. Transmittance modulation of EC devices at 550 nm for different TiO_2 thicknesses.

TiO_2 Thickness (nm)	ΔT (%)
95	21.3
83	25.7
63	26.9
48	38.3
32	23.1
16	15.4

For the same purpose, we varied the amount of silicon oil from 0 to 4 wt% in the precursor SnO_2 solution. Summarized in Table 3 is the measured ΔT value for different silicon oil concentrations. We found that the EC device without silicone oil had the lowest transmittance modulation of 4.4%. The ΔT value increased as the silicon oil concentration increased. It was due to the fact that the barrier layer prevents electrons from injecting into the EC layer, and at the same time, the accumulated holes in the EC layer promote the transport of the hydroxyl ions into the EC layer (Figure 13). A similar phenomenon (effect) was also demonstrated in a $WO_3/SiO_2/Ta_2O_5$ EC device fabricated by the sputtering process [21]. When the silicone oil concentration exceeds 3 wt% (thicker SiO_2 layer), the hydroxide ions do not easily move through the SiO_2 layer, degrading EC performance. Therefore, the optimum silicon oil concentration (SiO_2 layer thickness) was 3 wt% (~10 nm). With the optimum device structure (NiO doped with 2 wt% Sn, TiO_2 = 48 nm, SiO_2 = 10 nm), we achieved the transmittance modulation of as high as 38.3% and the coloration efficiency of 39.7 cm^2/C. Figure 15 shows the in situ transmittance curve during the continuous potential cycling test of the optimized EC device. The in situ transmittance change gradually degrades and then saturates at about 60,000 s, at which time the transmittance modulation is about 23%.

Table 3. Transmittance modulation of the EC device at 550 nm for different silicon oil concentrations.

Silicone Oil Concentration (wt%)	ΔT (%)
0	4.4
1	8.4
2	32.9
3	38.3
4	31.5

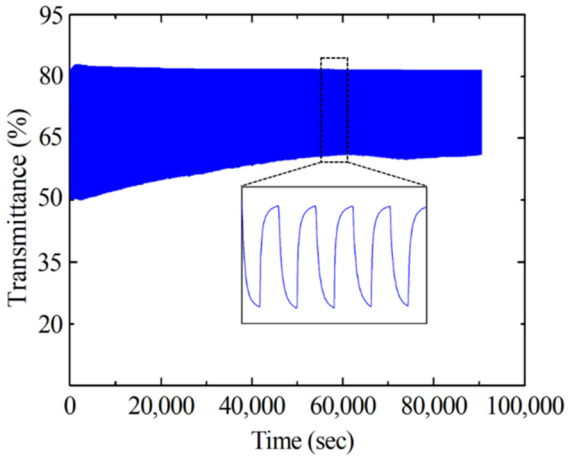

Figure 15. In situ transmittance curve during the continuous potential cycling test of the optimized EC device (NiO doped with 2 wt% Sn, TiO_2 = 48 nm, SiO_2 = 10 nm).

One of the main advantages of all-solid-state EC devices is their heat resistance. To demonstrate it, we measured the change in the ΔT value of the optimized EC device

(TiO_2 = 48 nm, SiO_2 = 10 nm, NiO doped with 2 wt% Sn), which is induced by the heat applied to the device using a hotplate for 2 hs. As evident in Figure 16, the ΔT value decreased with increasing temperature. The ΔT value was 38.3% at 25 °C, 33.2% at 60 °C, 24.6% at 100 °C, and 2.7% 140 °C. At 100 °C, the ΔT value was decreased by 36% from its initial value.

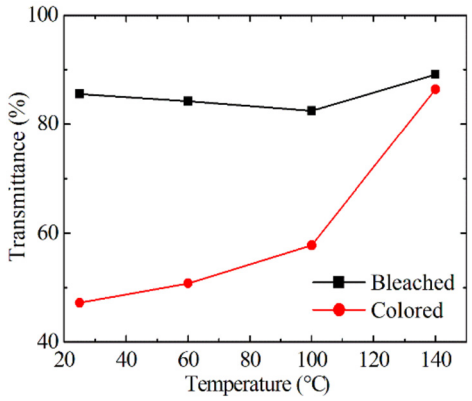

Figure 16. Transmittance in the bleached and colored states as a function of temperature.

3.3. Comparison between Spin and Slot Coatings

To demonstrate the scalability to large-area EC devices, we also fabricated the EC devices using slot-die coating under the same process condition described in Section 2.2.2. The thickness of each layer (SnO_2 = 61 nm, NiO = 30 nm) fabricated by slot-die coating was almost the same as that (SnO_2 = 62 nm, NiO = 32 nm) by spin coating. As shown in Figure 17, ΔT value was measured to be 34.1% (the transmittance of bleached and colored states was 80.7% and 46.6%, respectively), which was very close to that of the spin-coated EC device. We also made a comparison between them in terms of the surface morphology of the coated films. As seen in Figure 18 and Table 4, the surface morphology of the slot-coated SnO_2 on TiO_2 and NiO on SnO_2 was better than that of spin-coated films. The R_{pv} value (43 nm) of spin-coated SnO_2 was reduced to 16 nm by slot-die coating, and a similar effect was observed in the slot-coated NiO film. It was because more coating defects occur in spin coating, as evident in Figure 18e. Such a defect is attributed to that aggregation occurs or the film drying has progressed considerably under centrifugal force during spin coating. Therefore, slot-die coating can be employed in the fabrication of large-area all-solid-state EC devices without much compromise on the EC performance.

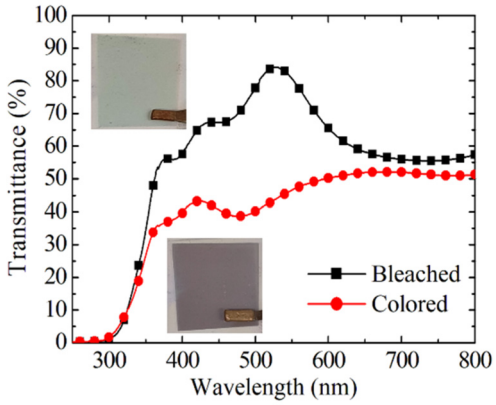

Figure 17. Transmittance spectra of the EC device fabricated by slot–die coating (the insets are photo images of the bleached and colored states).

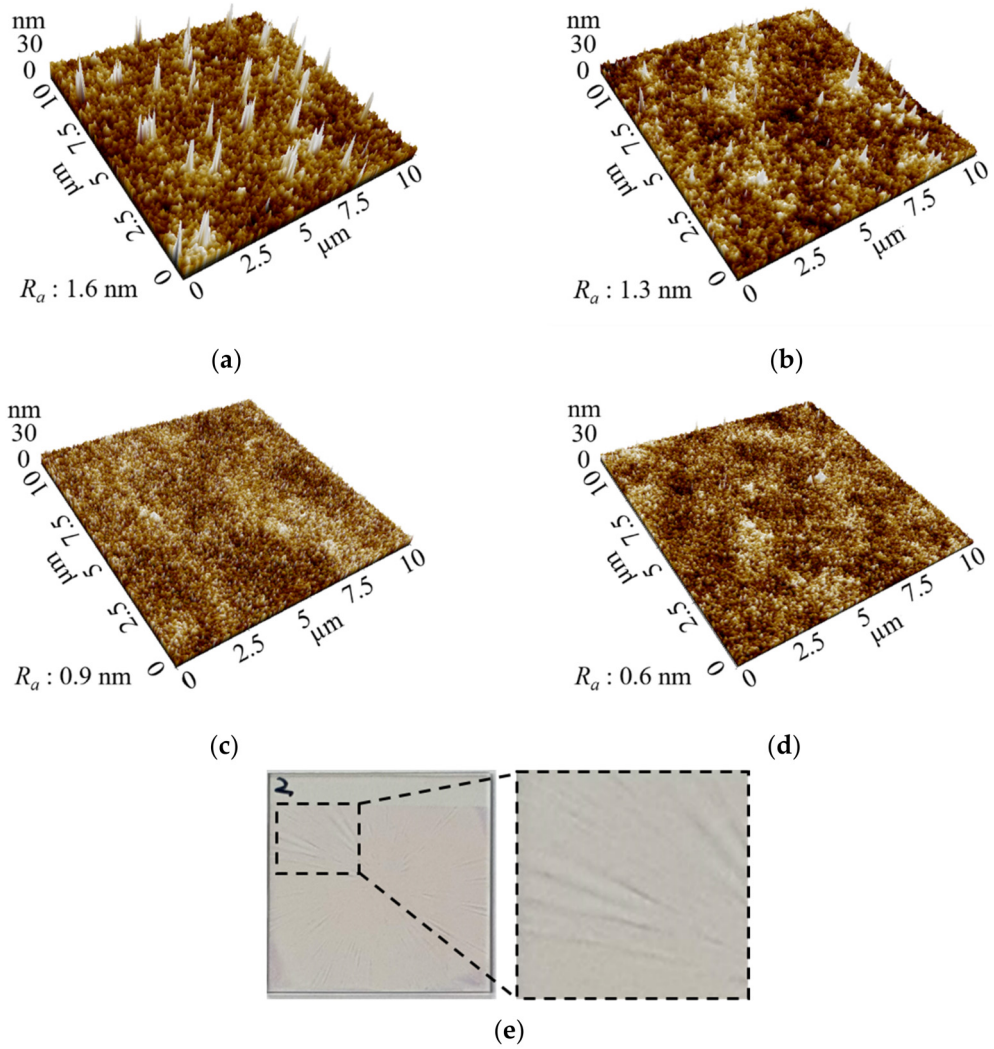

Figure 18. AFM images of (**a**) spin-coated SnO_2, (**b**) spin-coated NiO, (**c**) slot-coated SnO_2, (**d**) slot-coated NiO films, and (**e**) image of defects in the spin-coated SnO_2/NiO films.

Table 4. Surface roughness of spin/slot-coated SnO_2 on TiO_2 and NiO on SnO_2.

Layer	Spin Coating		Slot Coating	
	R_{pv} (nm)	R_a (nm)	R_{pv} (nm)	R_a (nm)
SnO_2	43	1.6	16	0.9
NiO	32	1.3	15	0.6

4. Conclusions

By a hybrid fabrication process (sputtering and sol-gel spin/slot coatings), we fabricated all-solid-state EC devices with Sn-doped NiO as an optically functional EC layer. It was found that the PC effect was enhanced from 7% to 29% and the EC effect from 5.1% to 25.7% by the addition of 2 wt% Sn into the precursor NiO solution. As a critical process for hydroxide-ion-based EC devices, UV/O_3 treatment was shown to enable (1) the formation of high-quality (dense and smooth) films, (2) the generation of hydroxide ions, (3) the conversion (phase separation) of silicon oil into the SiO_2 barrier at a low temperature, and (4) the enhancement of the overall device performance. The EC performance was also varied depending sensitively on the thickness of TiO_2 and SiO_2 layers, and the optimum thickness was 48 nm and 10 nm, respectively. With the optimum device structure (NiO doped with 2 wt% Sn, TiO_2 = 48 nm, SiO_2 = 10 nm), we achieved the transmittance modu-

lation of 38.3% and the coloration efficiency of 39.7 cm^2/C. The EC device also exhibited good heat resistance (36% decrease in the transmittance modulation at 100 °C for 2 h).

Author Contributions: Spin/slot-die coatings and measurement, G.K., S.H., and S.Y.; data analysis, writing, and supervision, J.P. All authors have read and agreed to the published version of the manuscript.

Funding: This research was supported by a building project of an innovative display process platform (20006469, "Development of roll to roll based manufacturing process and device application of transmittance variation smart film") funded by the Ministry of Trade, Industry and Energy.

Institutional Review Board Statement: Not applicable.

Informed Consent Statement: Not applicable.

Data Availability Statement: Not applicable.

Conflicts of Interest: The authors declare no conflict of interest.

References

1. Park, D. Optimization of Nickel Oxide-Based Electrochromic Thin Films. Ph.D. Thesis, Université Sciences et Technologies, Bordeaux, France, 2010.
2. Ohko, Y.; Tatsuma, T.; Fujii, T.; Naoi, K.; Niwa, C.; Kubota, Y.; Fujishima, A. Multicolour Photochromism of TiO_2 Films Loaded with Silver Nanoparticles. *Nat. Mater.* **2003**, *2*, 29–31. [CrossRef] [PubMed]
3. Liptay, W. Electrochromism and Solvatochromism. *Angew. Chemie Int. Ed. English* **1969**, *8*, 177–188. [CrossRef]
4. Li, W.; Zhang, X.; Chen, X.; Zhao, Y.; Wang, L.; Chen, M.; Zhao, J.; Li, Y.; Zhang, Y. Effect of Independently Controllable Electrolyte Ion Content on the Performance of All-Solid-State Electrochromic Devices. *Chem. Eng. J.* **2020**, *398*, 125628. [CrossRef]
5. Patel, K.J.; Bhatt, G.G.; Ray, J.R.; Suryavanshi, P.; Panchal, C.J. All-Inorganic Solid-State Electrochromic Devices: A Review. *J. Solid State Electrochem.* **2017**, *21*, 337–347. [CrossRef]
6. Aegerter, M.; Kim, C.Y. Dip-Coated TiO_2 CeO_2 Films as Transparent Counter-Electrode for Transmissive Electrochromic Devices Related Papers. *J. Non. Cryst. Solids* **1990**, *121*, 319–322. [CrossRef]
7. Özer, N.; Sabuncu, S.; Cronin, J. Electrochromic Properties of Sol-Gel Deposited Ti-Doped Vanadium Oxide Film. *Thin Solid Films* **1999**, *338*, 201–206. [CrossRef]
8. Azens, A.; Kullman, L.; Vaivars, G.; Nordborg, H.; Granqvist, C.G. Sputter-Deposited Nickel Oxide for Electrochromic Applications. *Solid State Ionics* **1998**, *113–115*, 449–456. [CrossRef]
9. Mehmood, A.; Long, X.; Haidry, A.A.; Zhang, X. Trends in Sputter Deposited Tungsten Oxide Structures for Electrochromic Applications: A Review. *Ceram. Int.* **2020**, *46*, 23295–23313. [CrossRef]
10. Joost, U.; Šutka, A.; Oja, M.; Smits, K.; Döbelin, N.; Loot, A.; Järvekülg, M.; Hirsimäki, M.; Valden, M.; Nõmmiste, E. Reversible Photodoping of TiO_2 Nanoparticles for Photochromic Applications. *Chem. Mater.* **2018**, *30*, 8968–8974. [CrossRef]
11. Pittaluga, M. *Eco-efficient Materials for Mitigating Building Cooling Needs*; Woodhead Publishing: Cambridge, UK, 2015; pp. 473–497. [CrossRef]
12. Sta, I.; Jlassi, M.; Hajji, M.; Ezzaouia, H. Structural, Optical and Electrical Properties of Undoped and Li-Doped NiO Thin Films Prepared by Sol-Gel Spin Coating Method. *Thin Solid Films* **2014**, *555*, 131–137. [CrossRef]
13. Ren, Y.; Chim, W.K.; Guo, L.; Tanoto, H.; Pan, J.; Chiam, S.Y. The Coloration and Degradation Mechanisms of Electrochromic Nickel Oxide. *Sol. Energy Mater. Sol. Cells* **2013**, *116*, 83–88. [CrossRef]
14. Nundy, S.; Mesloub, A.; Alsolami, B.M.; Ghosh, A. Electrically Actuated Visible and Near-Infrared Regulating Switchable Smart Window for Energy Positive Building: A Review. *J. Clean. Prod.* **2021**, *301*, 126854. [CrossRef]
15. Koo, J.; Amoli, V.; Kim, S.Y.; Lee, C.; Kim, J.; Park, S.M.; Kim, J.; Ahn, J.M.; Jung, K.J.; Kim, D.H. Low-Power, Deformable, Dynamic Multicolor Electrochromic Skin. *Nano Energy* **2020**, *78*, 105199. [CrossRef]
16. Macrelli, G. Optical Characterization of Commercial Large Area Liquid Crystal Devices. *Sol. Energy Mater. Sol. Cells* **1995**, *39*, 123–131. [CrossRef]
17. Piccolo, A.; Pennisi, A.; Simone, F. Daylighting Performance of an Electrochromic Window in a Small Scale Test-Cell. *Sol. Energy* **2009**, *83*, 832–844. [CrossRef]
18. Yang, H.; Wang, C.; Diao, X.; Wang, H.; Wang, T.; Zhu, K. A New All-Thin-Film Electrochromic Device Using LiBSO as the Ion Conducting Layer. *J. Phys. D. Appl. Phys.* **2008**, *41*. [CrossRef]
19. Song, X.; Dong, G.; Gao, F.; Xiao, Y.; Liu, Q.; Diao, X. Properties of NiO_x and Its Influence upon All-Thin-Film ITO/NiO_x/$LiTaO_3$/WO_3/ITO Electrochromic Devices Prepared by Magnetron Sputtering. *Vacuum* **2015**, *111*, 48–54. [CrossRef]
20. Li, W.; Zhang, X.; Chen, X.; Zhao, Y.; Wang, L.; Liu, D.; Li, X.; Chen, M.; Zhao, J.; Li, Y. Preparation and Performance of Fast-Response ITO/Li-NiO/Li-WO_3/ITO All-Solid-State Electrochromic Devices by Evaporation Method. *Mater. Lett.* **2020**, *265*, 127464. [CrossRef]

21. Yoshimura, H.; Koshida, N. Fast Electrochromic Effect Obtained from Solid-State Inorganic Thin-Film Configuration with a Carrier Accumulation Structure. *Appl. Phys. Lett.* **2006**, *88*, 86–89. [CrossRef]
22. Wang, S.C.; Liu, K.Y.; Huang, J.L. Tantalum Oxide Film Prepared by Reactive Magnetron Sputtering Deposition for All-Solid-State Electrochromic Device. *Thin Solid Films* **2011**, *520*, 1454–1459. [CrossRef]
23. Kim, K.H.; Kahuku, M.; Abe, Y.; Kawamura, M.; Kiba, T. Improved Electrochromic Performance in Nickel Oxide Thin Film by Zn Doping. *Int. J. Electrochem. Sci.* **2020**, *15*, 4065–4071. [CrossRef]
24. Patil, P.S.; Sadale, S.B.; Mujawar, S.H.; Shinde, P.S.; Chigare, P.S. Synthesis of Electrochromic Tin Oxide Thin Films with Faster Response by Spray Pyrolysis. *Appl. Surf. Sci.* **2007**, *253*, 8560–8567. [CrossRef]
25. Azevedo, C.F.; Balboni, R.D.C.; Cholant, C.M.; Moura, E.A.; Lemos, R.M.J.; Pawlicka, A.; Gündel, A.; Flores, W.H.; Pereira, M.; Avellaneda, C.O. New Thin Films of NiO Doped with V_2O_5 for Electrochromic Applications. *J. Phys. Chem. Solids* **2017**, *110*, 30–35. [CrossRef]
26. Takaki, H.; Inoue, S.; Matsumura, Y. Requirements for Photochromism in Double-Layer Metal Oxide Films. *Chem. Phys. Lett.* **2019**, *732*, 136620. [CrossRef]
27. Wang, K.; Zhang, H.; Xie, W.; Chen, G.; Jiang, R.; Tao, K.; Liang, L.; Gao, J.; Cao, H. Unraveling the Role of Water on the Electrochromic and Electrochemical Properties of Nickel Oxide Electrodes in Electrochromic Pseudocapacitors. *J. Electrochem. Soc.* **2021**, *168*, 113502. [CrossRef]
28. Sawaby, A.; Selim, M.S.; Marzouk, S.Y.; Mostafa, M.A.; Hosny, A. Structure, Optical and Electrochromic Properties of NiO Thin Films. *Phys. B Condens. Matter* **2010**, *405*, 3412–3420. [CrossRef]
29. Tachikawa, H.; Abe, S. Spectral Shifts of Ozone Molecule by the Complex Formation with a Water Molecule. *Chem. Phys. Lett.* **2006**, *432*, 409–413. [CrossRef]
30. Noonuruk, R.; Wongpisutpaisan, N.; Mukdacharoenchai, P.; Techitdheera, W.; Pecharapa, W. Ozone-Induced Optical Density Change of NiO Thin Films and Their Applicability as Neutral Optical Density Filter. *Procedia Eng.* **2011**, *8*, 212–216. [CrossRef]
31. Méndez, P.F.; Muhammed, S.K.M.; Barea, E.M.; Masi, S.; Mora-Seró, I. Analysis of the UV–Ozone-Treated SnO_2 Electron Transporting Layer in Planar Perovskite Solar Cells for High Performance and Reduced Hysteresis. *Sol. RRL* **2019**, *3*, 1–6. [CrossRef]
32. Wang, K.; Qiu, D.; Zhang, H.; Chen, G.; Xie, W.; Tao, K.; Bao, S.; Liang, L.; Gao, J.; Cao, H. Boosting Charge-Transfer Kinetics and Cyclic Stability of Complementary WO_3–NiO Electrochromic Devices via SnOx Interfacial Layer. *J. Sci. Adv. Mater. Devices* **2021**, *6*, 494–500. [CrossRef]
33. Lin, T.; Li, X.; Jang, J. High Performance P-Type NiOx Thin-Film Transistor by Sn Doping. *Appl. Phys. Lett.* **2016**, *108*. [CrossRef]
34. Ouyang, M.; Yuan, C.; Muisener, R.J.; Boulares, A.; Koberstein, J.T. Conversion of Some Siloxane Polymers to Silicon Oxide by UV/Ozone Photochemical Processes. *Chem. Mater.* **2000**, *12*, 1591–1596. [CrossRef]
35. Shi, J.; Lai, L.; Zhang, P.; Li, H.; Qin, Y.; Gao, Y.; Luo, L.; Lu, J. Aluminum Doped Nickel Oxide Thin Film with Improved Electrochromic Performance from Layered Double Hydroxides Precursor in Situ Pyrolytic Route. *J. Solid State Chem.* **2016**, *241*, 1–8. [CrossRef]
36. Jung, K.; Kim, D.H.; Kim, J.; Ko, S.; Choi, J.W.; Kim, K.C.; Lee, S.G.; Lee, M.J. Influence of a UV-Ozone Treatment on Amorphous SnO_2 Electron Selective Layers for Highly Efficient Planar $MAPbI_3$ Perovskite Solar Cells. *J. Mater. Sci. Technol.* **2020**, *59*, 195–202. [CrossRef]